Available online at www.sciencedirect.com
ScienceDirect
Journal of Solid State Chemistry 179 (2006) 3805–3813
JOURNAL OF SOLID STATE CHEMISTRY
www.elsevier.com/locate/jssc

Structural manipulation of pyrochlores: Thermal evolution of metastable $Gd_2(Ti_{1-y}Zr_y)_2O_7$ powders prepared by mechanical milling

Karla J. Moreno[a], Antonio F. Fuentes[a,*], Miroslaw Maczka[b], Jerzy Hanuza[b,c], Ulises Amador[d]

[a]*Cinvestav-Saltillo, Apartado Postal 663, 25000-Saltillo, Coahuila, Mexico*
[b]*Institute of Low Temperature and Structure Research, Polish Academy of Sciences, PO Box 1410, 50-950 Wroclaw 2, Poland*
[c]*Department of Bioorganic Chemistry, Faculty of Engineering and Economics, University of Economics, Wroclaw, Poland*
[d]*Departamento de Química, Facultad de Farmacia, Universidad San Pablo CEU, 28668-Boadilla del Monte, Madrid, Spain*

Received 7 June 2006; received in revised form 25 July 2006; accepted 21 August 2006
Available online 25 September 2006

Abstract

The structural and microstructural characteristics of metastable $Gd_2(Ti_{1-y}Zr_y)_2O_7$ powders prepared by mechanical milling have been studied by a combination of XRD and Raman spectroscopy. Irrespective of their Zr content, as-prepared powder phases present an anion-deficient fluorite-type of structure as opposed to the pyrochlore equilibrium configuration obtained for the same solid solution by other synthetic routes. These fluorites are stable versus thermal activation, at least up to temperatures of 800 °C. For the Ti-rich compositions, thermal treatments at higher temperatures facilitate the rearrangement of the cation and anion substructures and the relaxation of mechanochemically induced defects whereas for compositions with high Zr content, the fluorite crystal structure is retained even at temperatures as high as 1200 °C. Interestingly enough, transient pyrochlores showing a very unusual cation distribution were observed during the thermally induced defect-recovery process.

Keywords: Mechanical milling; Raman spectroscopy; Defect fluorites; Order–disorder; Pyrochlores

1. Introduction

The conventional solid state synthesis technology, consisting of long firing cycles at high temperatures provides poor control of morphology and particle size and produces undesirable characteristics in the final product such as phase and stoichiometric heterogeneities. Although alternative routes have been proposed over the years to increase reaction rates and/or to decrease reaction temperatures, more than often they also require thermal treatments for the formation or crystallization of the desired product. Mechanical milling which was conceived initially to synthesize nanocrystalline metals and powder alloys [1] has found in recent years application in different areas of materials science of technological interest. Thus, it has been used for mineral and waste processing, ultrafine powder production, synthesis of novel crystalline phases, preparation of a fine dispersion of second-phase particles or extended solid solutions [2]. As a far-from-equilibrium processing method, mechanical milling allows also the room-temperature preparation of metastable phases existing at equilibrium only at high temperature and/or high pressure frequently leading to unique defect structures difficult to obtain or even unattainable by any other synthetic route. In fact, the departure from equilibrium which is possible to reach using mechanochemical processes has been estimated to be comparable to that obtained with irradiation/ion implantation (ballistic interactions) [2]. Additional processing (e.g. post-milling thermal treatments) offers the possibility of manipulating the structural and/or microstructural characteristics of the target phase and therefore, tuning a given property to a specific need.

Pyrochlore oxides $A_2B_2O_7$ are a very interesting family of compounds showing a large variety of physical and

*Corresponding author. Fax: +52 8444389610.
E-mail address: antonio.fernandez@cinvestav.edu.mx (A.F. Fuentes).

0022-4596/$ - see front matter © 2006 Elsevier Inc. All rights reserved.
doi:10.1016/j.jssc.2006.08.023

chemical properties depending on chemical composition and the existing ordering (disordering) of the *A* and *B*-site cations and oxygen vacancies. Thus, some pyrochlores are ionic, electronic or mixed conductors [3] or show unusual magnetic properties [4,5]. Because of their ability to accept rare earth elements in solid solutions and their chemical and thermal stability, they are even currently considered as important ceramic waste forms for the immobilization of high-level radioactive waste [6]. The fully ordered or "ideal" pyrochlore with $A_2B_2X_6Y$ stoichiometry, such as $Gd_2Ti_2O_6O'$, presents cubic symmetry (S.G.: $Fd\bar{3}m$) and can be described in terms of a superstructure of the ideal defect fluorite structure (cubic, S.G.: $Fm\bar{3}m$) with twice the cell constant, $a \approx 10$ Å (see Ref. [7] for a detailed description of the pyrochlore crystal structure). The eight-coordinated *A*-site (16*c*) located at the center of a scalenohedron, is normally occupied by the larger cation whereas the six-coordinated *B*-site (16*d*) located at the center of a trigonal antiprism, is usually occupied by the smaller cation. The *X* anions occupy the 48*f* site coordinated to two B^{4+} and two A^{3+} cations while the *Y* anions occupy the 8*a* site being tetrahedrally coordinated to four A^{3+} cations. Additionally, there is another anionic tetrahedral site (8*b*) coordinated to four B^{4+} ions, which is systematically vacant in ordered pyrochlores. Thus, while vacancies are randomly distributed throughout the anion substructure in fluorites, they are ordered in particular sites in "ideal" pyrochlores. There are also pyrochlores referred to as "defect" pyrochlores, such as $Gd_2Zr_2O_7$, which present a partially disordered atomic array. The structural phase transition from pyrochlore to the ideal defect fluorite involves the randomization of the anions among the 48*f*, 8*a* and 8*b* sites (becoming the 8*c* site in fluorites) and that of the cations among the 16*c* and 16*d* sites (the 4*a* site in fluorites) with different degrees of disorder being possible in systems of solid solutions by using the appropriate substitutions on the *A*- and *B*-sites. Thus, atomic disordering in the $Gd_2(Ti_{1-y}Zr_y)_2O_7$ solid solution increases as Zr content increases by a combination of oxygen Frenkel and cation antisite defects, although complete randomization in equilibrium configurations is never reached [8,9]. Thus, $Gd_2Zr_2O_7$ presents at room-temperature a "defect" pyrochlore type of structure and only when fired above 1500 °C transforms itself into an anion-deficient fluorite-type of structure [10]. As it has been already shown [11], mechanical milling allows preparation of metastable partially disordered $RE_2Ti_2O_7$ pyrochlores obtained otherwise only by chemical substitution or by ion irradiation [8,12]. In this paper, we will analyze the effect of processing $Gd_2(Ti_{1-y}Zr_y)_2O_7$ pyrochlore oxides which are intrinsically disordered, by mechanical milling and will follow their evolution with post-milling thermal treatments.

2. Experimental

Three compositions within the title solid solution with different Zr/Ti ratios, $Gd_2(Ti_{0.65}Zr_{0.35})_2O_7$, $Gd_2(Ti_{0.35}Zr_{0.65})_2O_7$ and $Gd_2(Ti_{0.10}Zr_{0.90})_2O_7$, were prepared as described elsewhere [13], by dry milling stoichiometric mixtures of the constituent oxides (high purity monoclinic ZrO_2, anatase-TiO_2 and C-Gd_2O_3), in a planetary ball mill using zirconia vials and balls. Portions of these powder samples were subjected to post-milling thermal treatments (12 h) at temperatures between 400 and 1200 °C and analyzed by X-ray powder diffraction and Raman spectroscopy. The structural and microstructural features of the as prepared materials were obtained from precise diffraction data obtained on a Bruker D8 high-resolution X-ray powder diffractometer equipped with a position sensitive detector (PSD) MBraun PSD-50M, using monochromatic $CuK_{\alpha 1}$ radiation ($\lambda = 1.5406$ Å) obtained with a germanium primary monochromator. The measured angular range, the step size and counting times were selected to ensure enough resolution (the step size should be at least, 1/10 of the fwhms) and statistics. The instrumental contribution to line broadening was evaluated using NIST LaB_6 standard reference material (SRM 660a; $\mu = 1138\,cm^{-1}$, linear absorption coefficient for $CuK_{\alpha 1}$ radiation). The structural refinements were carried out by the Rietveld method using the FullProf program [14] and taking into account, simultaneously, the effects of the sample microstructure on the diffraction patterns according to a phenomenological approach described in detail elsewhere [15]. Raman spectra were recorded with a Bruker FT-Raman RFS 100/S spectrometer. Excitation was performed with a YAG:Nd^{3+} laser and the spectral resolution was $2\,cm^{-1}$.

3. Results and discussion

3.1. Structural characterization by XRD

Figs. 1a and 1b show graphically, the fitting result of two X-ray diffraction patterns corresponding to the as prepared $Gd_2(Ti_{0.10}Zr_{0.90})_2O_7$ powders, milled and fired 12 h at 400 and 1200 °C, respectively. As the pyrochlore structure can be considered as a superstructure of an anion-deficient fluorite-like atomic arrangement, its diffraction pattern contains a set of strong intensities characteristic of the underlying fluorite-type substructure cell plus an additional set of superstructure reflections with intensities depending on factors such as the degree of ordering, difference in the average scattering factors of the elements involved, distribution of oxygen vacancies, etc [3]. Since no superstructure peaks corresponding to the pyrochlore long-range atomic ordering, are observed in Fig. 1, the first observation to point out is that both samples consist of fluorite-like materials. The results of the structural refinement of this series of Zr-rich samples are collected in Table 1 together with their microstructural features obtained from the Langford plots [16–18]. Thus, this composition maintains the defect fluorite-type of structure even after 12 h firing at 1200 °C, with cell parameters remaining almost temperature independent (only some

0.1% change along the whole series). On the contrary, similar titanates obtained by ball milling but with a partially disordered pyrochlore-type of structure [11] show different cell volumes (decreasing with increasing firing temperature) depending on the cation distribution between the two positions available. As observed when samples in the title solid solution were prepared by other routes [8,9], the tendency to adopt a pyrochlore structure in samples prepared by mechanical milling increases as the Ti content increases. Thus, while the series of samples of composition $Gd_2(Ti_{0.35}Zr_{0.65})_2O_7$ just-milled and treated at temperatures of up to 1000 °C retain the fluorite structure (Fig. 2a and Table 2), that treated at high temperature (1200 °C) shows an XRD pattern typical of a pyrochlore-like material. In Fig. 2b the superstructure peaks, $(hkl)_p$ with h, k and l odd, due to the cation (and anion) ordering present in pyrochlore, are observed (i.e. the (331) line in the inset of Fig. 2b). As before, all the fluorite-like compounds of this series have also similar unit cell parameters (Table 2). However, the metal distribution between the large and eight-coordinated 16*c* site and the smaller and hexa-coordinated 16*d* site in the pyrochlore $Gd_2(Ti_{0.35}Zr_{0.65})_2O_7$ fired at 1200 °C is very much unexpected. Based on metal ions size, one would expect the 16*c* site to be fully occupied by the larger Gd^{3+} ions whereas the smaller Ti^{4+} and Zr^{4+} ions would share the hexa-coordinated position (16*d*) ($r(Ti^{4+}) = 0.61$ Å, $r(Zr^{4+}) = 0.72$ Å, $r(Gd^{3+}) = 0.94$ Å, all in octahedral coordination) [19]. However, it was evident along the XRD data fitting that an important fraction of Gd ions were located at the hexa-coordinated 16*d* sites (about 75% in the final step of the fitting process) driving in consequence, all the Zr^{4+} atoms and some Ti^{4+} ions to the 16*c* sites. At this point, it is worth explaining how we arrived to the cation distribution presented in Table 2. As a starting model, we assumed all the Gd ions to be constrained into the 16*c* sites and correspondingly, the existing Ti and Zr ions sharing the 16*d* position but it was evident during the fitting process that much more scattering power should be located in the 16*d* sites. This could only be accomplished by allowing Gd ions to move into the latter and consequently, removing either Ti or Zr. From crystallochemical considerations, the obvious choice was Zr. Thus, we refined the occupation of both sites allowing Zr to move to the 16*c* sites and Gd to occupy the octahedral sites. However, even after placing all the Zr

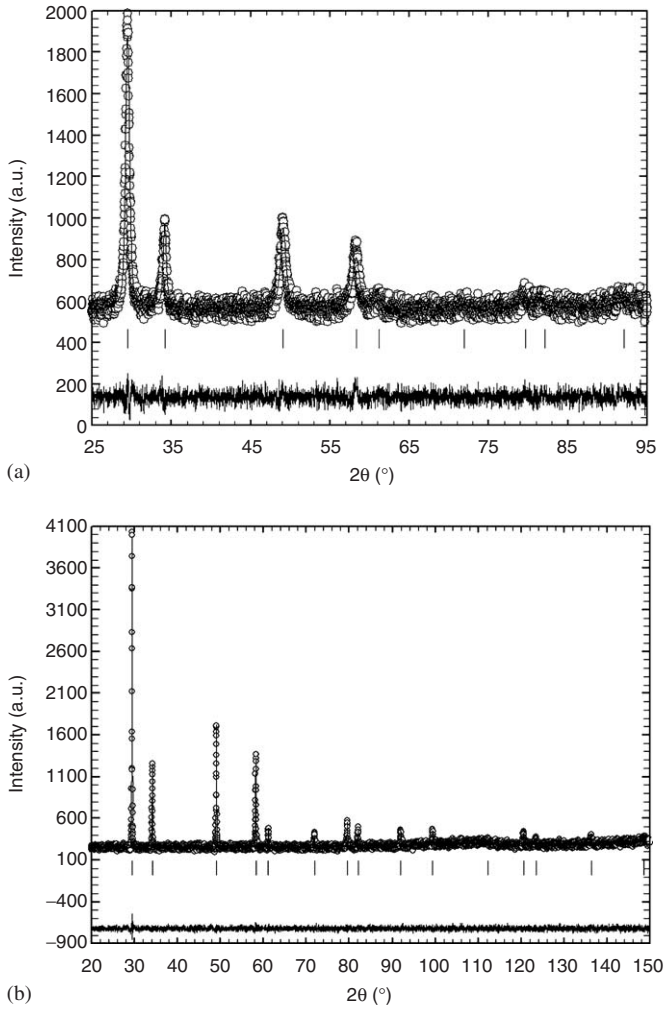

Fig. 1. Experimental (points), calculated (solid line) and difference (bottom) X-ray diffraction patterns for a $Gd_2(Ti_{0.10}Zr_{0.90})_2O_7$ powder sample after ball milling 19 h at RT and a post-milling thermal treatment for 12 h at 400 °C (a) and at 1200 °C (b).

Table 1
Selected structural and microstructural parameters for the as-prepared $Gd_2(Ti_{0.10}Zr_{0.90})_2O_7$ powder samples submitted to post-milling thermal treatments at different temperatures

Treatment T(°C)/time (h)	No treatment	400/12	600/12	800/12	1000/12	1200/12
Structural type symmetry	Fluorite *Fm*3*m* (*n*. 225)					
a (Å)	5.2406(9)	5.2454(6)	5.246(1)	5.2447(4)	5.2486(4)	5.2482(1)
Gd/Ti/Zr in 4*a*, *m*3*m*, (0 0 0), Occ.	0.5/0.05/0.45					
O(1) in 8*c*, −43*m* ($\frac{1}{4}\frac{1}{4}\frac{1}{4}$), Occ.	7/8					
R_B	0.082	0.026	0.075	0.049	0.052	0.026
R_{wp}	0.052	0.043	0.089	0.043	0.048	0.061
R_{exp}	0.036	0.041	0.084	0.040	0.041	0.056
χ^2	2.10	1.10	1.12	1.12	1.37	1.17
[b] $\langle D_{iso} \rangle$ (Å)	65(10)	95(15)	167(13)	100(10)	230(20)	1030(90)
[c] e_{rms}	4(3) 10^{-3}	8(2) 10^{-3}	11(5) 10^{-3}	2.9(5) 10^{-3}	3(1) 10^{-3}	8(1) 10^{-4}

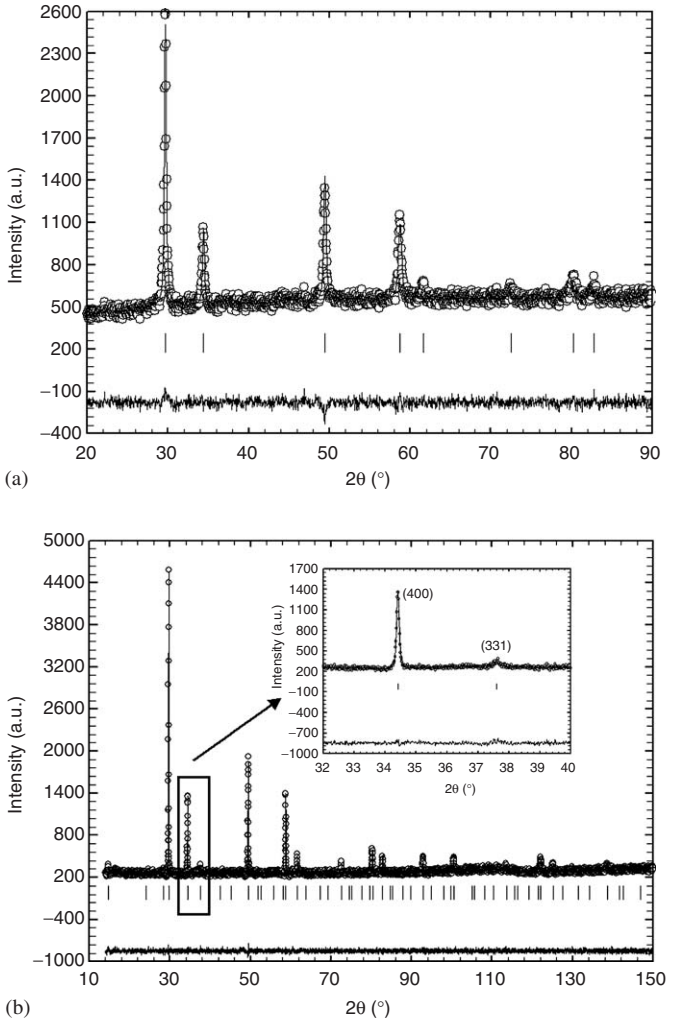

Fig. 2. Experimental (points), calculated (solid line) and difference (bottom) X-ray diffraction patterns for the as-prepared $Gd_2(Ti_{0.35}Zr_{0.65})_2O_7$ powder sample and after a post-milling thermal treatment for 12 h at 1000 °C (a) and at 1200 °C (b). In the inset of (b) a zone of the pattern is magnified to show the relative intensity of pyrochlore superstructure peaks (see text).

atoms into the eight-coordinated position, some scattering power was still missing in the 16*d* site. We carry on then allowing some Ti ions into the 8-coordinated site and more Gd atoms to enter the 16*d* site. The final refined distribution is that presented in Table 2. Although other cation distributions could be possible (formally the number of unknowns is larger than the information available), they were discarded on the basis of crystallochemical considerations and for being artificially and unnecessarily complex. The satisfactory fitting of the XRD data together with the Raman spectra (see next section) confirm the starting hypothesis about cation distribution. Hence, mechanochemically prepared $Gd_2(Ti_{0.35}Zr_{0.65})_2O_7$ presents at room-temperature a fluorite-type of structure stable up to at least 1000 °C with thermal treatments at higher temperatures (1200 °C) allowing a partial redistribution of cations. It seems that the equilibrium cation distribution has not been reached even at this temperature, i.e. this configuration is an intermediate step in the rearrangement of ions towards the thermodynamically stable structure, more temperature and/or time being needed to reach the stable state.

The key for understanding the mechanism involved in the thermally induced fluorite-to- pyrochlore phase transformation on samples prepared by mechanical milling is given by the series of samples with composition $Gd_2(Ti_{0.65}Zr_{0.35})_2O_7$. It is important to remember that a remarkable increase in ionic conductivity is observed in the title solid solution for compositions containing ~30% of the Ti atoms replaced by Zr, which has been related with the onset of anion disordering [8]. Therefore, this series lies close to the boundary between the fully ordered "ideal" and the "defect" pyrochlore stability fields found in $Gd_2(Ti_{1-y}Zr_y)_2O_7$ for equilibrium phases. As Table 3 shows, the samples of this Ti-rich series treated at low temperature (up to 800 °C) retain the fluorite-type of structure with as before, cell parameters remaining almost independent of the temperature of post-milling thermal treatments (Table 3). However, samples treated at higher temperatures (1000 and 1200 °C) present XRD patterns (not shown) typical of pyrochlore-like materials although their cation distribution is quite different as evidenced by the relative intensity of the superstructure peaks. As the structure factor (F_{hkl}) of the superstructure peaks depends on the difference of scattering power between the 16*c* and the 16*d* sites and that of the peaks with *h*, *k* and *l* even depends on the addition of the scattering power in both positions (constant along the whole series as the composition is), the relative intensity of the superstructure peaks is a direct evidence of the cation distribution in the structure. The site occupancies given in Table 3 have been obtained by a procedure similar to that described above for the pyrochlore of the previous series (Table 2). In fact, we used this as a starting model to fit the XRD data of the sample $Gd_2(Ti_{0.65}Zr_{0.35})_2O_7$ treated at 1000 °C. As a common feature, Zr atoms in both phases are not found in the 16*d* sites while the majority of the Ti ions are located in these hexa-coordinated positions; as for Gd, their differences in chemical composition make for a different distribution. In the sample heated at higher temperature (1200 °C) the cations tend to occupy their "natural" sites. Thus, all the Ti atoms are now located in the 16*d* sites, Gd ions move to a large extent (80%) to the 16*c* sites and Zr ions are equally split between both.

What about the anion substructure? Since X-ray diffraction techniques are not adequate to study structural features related to light atoms such as oxygen, the oxygen array in our structural refinements (Tables 1–3) is assumed to be ordered as in the ideal pyrochlore structure, whereas in fluorite 1/8 of the oxygen positions are empty at random. In what follows we will present also the characterization of our samples by Raman spectroscopy, better suited to provide information about the anion substructure.

Table 2
Selected structural and microstructural parameters for the as-prepared $Gd_2(Ti_{0.35}Zr_{0.65})_2O_7$ powder samples submitted to post-milling thermal treatments at different temperatures

Treatment T(°C) time (h)	No treatment	400/12	600/12	800/12	1000/12		1200/12
Structural type symmetry	Fluorite *Fm*3*m* (*n*. 225)						Pyrochlore *Fd*3*m* (*n*. 227)
a (Å)	5.206(3)	5.212(2)	5.217(3)	5.2141(9)	5.2093(8)	*a* (Å)	10.4154(1)
Gd/Ti/Zr in 4*a*,*m*3 *m*, (0 0 0), Occ.			0.5/0.175/0.325			Gd/Zr/Ti in 16c, −3 m, (0 0 0), Occ.	0.26(1)/0.65/0.09(1)
O(1) in 8*c*, –43 *m* ($\frac{1}{4}\frac{1}{4}\frac{1}{4}$), Occ.			7/8			Gd/Ti in 16d, −3 m, ($\frac{1}{2}\frac{1}{2}\frac{1}{2}$), Occ.	0.74(1)/0.26(1)
						O(1) in 48f, mm (× 1/8 1/8), Occ.	1
						x	0.416(1)
						O(2) in 8a, −43 m, (1/8 1/8 1/8), Occ.	1
R_B	0.035	0.030	0.082	0.019	0.036		0.044
R_{wp}	0.043	0.037	0.082	0.036	0.072		0.060
R_{exp}	0.036	0.035	0.078	0.034	0.071		0.058
χ^2	1.42	1.15	1.11	1.18	1.03		1.11
[(b)] $\langle D_{iso} \rangle$ (Å)	82(13)	78(25)	133(9)	107(21)	202(54)		187(2)
[(c)] e_{rms}	6(6) 10^{-3}	8(6) 10^{-3}	9(3) 10^{-3}	7(2) 10^{-3}	4(2) 10^{-3}		1.7(8) 10^{-3}

Table 3
Selected structural and microstructural parameters for the as-prepared $Gd_2(Ti_{0.65}Zr_{0.35})_2O_7$ powder samples submitted to post-milling thermal treatments at different temperatures

Treatment T(°C)/ time (h)	No treatment	600/12	800/12		1000/12	1200/12
Structural type symmetry	Fluorite *Fm*3*m* (*n*. 225)				Pyrochlore *Fd*3*m* (*n*. 227)	
a (Å)	5.160(6)	5.179(2)	5.1698(7)	*a* (Å)	10.3208(2)	10.3171(1)
Gd/Ti/Zr in 4*a*, *m*3 *m*, (0 0 0), Occ.		0.5/0.325/0.175		Gd/Zr/Ti in 16c, −3 m, (0 0 0), Occ.	0.57(2)/0.35/0.08(2)	0.80(2)/0.20(2)/0.0
O(1) in 8*c*, –43*m* ($\frac{1}{4}\frac{1}{4}\frac{1}{4}$), Occ.		7/8		Gd/Zr/Ti in 16d, −3 m, (($\frac{1}{2}\frac{1}{2}\frac{1}{2}$)), Occ.	0.43(2)/0.0/0.57(2)	0.20(2)/0.15(2)/0.65
				O(1) in 48f, mm (x 1/8 1/8), Occ.	1	
				x	0.415(2)	0.417(1)
				O(2) in 8a, −43 m, (1/8 1/8 1/8), Occ.	1	
R_B	0.064	0.068	0.048		0.054	0.055
R_{wp}	0.056	0.051	0.034		0.050	0.062
R_{exp}	0.054	0.050	0.029		0.047	0.059
χ^2	1.05	1.02	1.33		1.12	1.13
[(b)] $\langle D_{iso} \rangle$ (Å)	63(30)	74(9)	150(20)		145(4)	284(20)
[(c)] e_{rms}	5(3) 10^{-3}	6(4) 10^{-3}	5(1) 10^{-3}		3(2) 10^{-3}	1(1) 10^{-4}

3.2. Raman spectroscopy

Previous studies on characterization of $Gd_2(Ti_{1-y}Zr_y)_2O_7$ powders prepared by sintering of oxides at high temperatures as well as of partially disordered $RE_2Ti_2O_7$ pyrochlores (RE = Gd, Y, Dy) prepared by mechanical milling from constituent oxides, have shown Raman spectroscopy to give valuable information about oxygen disorder [9,11,20]. Thus, it has been shown that displacement of oxygen ions toward the vacant 8*b* site in the pyrochlore structure, gives rise to the development of a new and broad Raman band near 750 cm^{-1} which was assigned to seven-coordinated Ti atoms [9,20]. It was also observed that increasing disorder produces a few other characteristic changes in the Raman spectra; i.e. significant broadening of bands, shift of the 519 cm^{-1} (A_{1g}), 549 cm^{-1} (F_{2g}) and 312 cm^{-1} (E_g) bands towards higher frequency, shift of the 455 cm^{-1} (F_{2g}) band towards lower frequency, and intensity increase of the 549 and 455 cm^{-1} bands [9]. Thus, increasing disorder with increasing concentration of Zr^{4+} ions was very clearly observed for the

$Gd_2(Ti_{1-y}Zr_y)_2O_7$ series. When a defect fluorite structure was reached for pure $Gd_2Zr_2O_7$, only four bands were observed at 597, 543, 407 and 318 cm^{-1} [9]. In our case, the spectrum obtained for the $Gd_2(Ti_{0.10}Zr_{0.90})_2O_7$ sample fired at 1200 °C (not shown) is in very good agreement with the spectrum of defect fluorite-type $Gd_2Zr_2O_7$ presented by Hess et al. [9]. Interestingly enough, the only difference is the presence in our sample of a band near 750 cm^{-1} assigned to seven-coordinated titanium atoms. Therefore, as observed by XRD, Raman spectroscopy shows that even when fired at high temperature, our $Gd_2(Ti_{0.10}Zr_{0.90})_2O_7$ series of samples presents a defect fluorite-type of structure. The Raman spectra obtained for the $Gd_2(Ti_{0.35}Zr_{0.65})_2O_7$ powders treated at 400 and 800 °C (not shown) are also similar to that characteristic of fluorite-type materials although the intensity of the band near 750 cm^{-1} increased strongly which is attributed to increased concentration of Ti^{4+}. The sample treated at 1000 °C still shows the presence of the same three bands characteristic of the fluorite structure. However, the intensity of the band near 750 cm^{-1} decreases significantly (decreasing number of seven-coordinated Ti ions) indicating some kind of atomic rearrangement starting at this temperature although this atomic ordering must be of short-range since the XRD study of this sample does not indicate the presence of any superlattice reflection characteristic of the pyrochlore structure. Fig. 3 shows the Raman spectra obtained for the Ti-rich series, $Gd_2(Ti_{0.65}Zr_{0.35})_2O_7$,

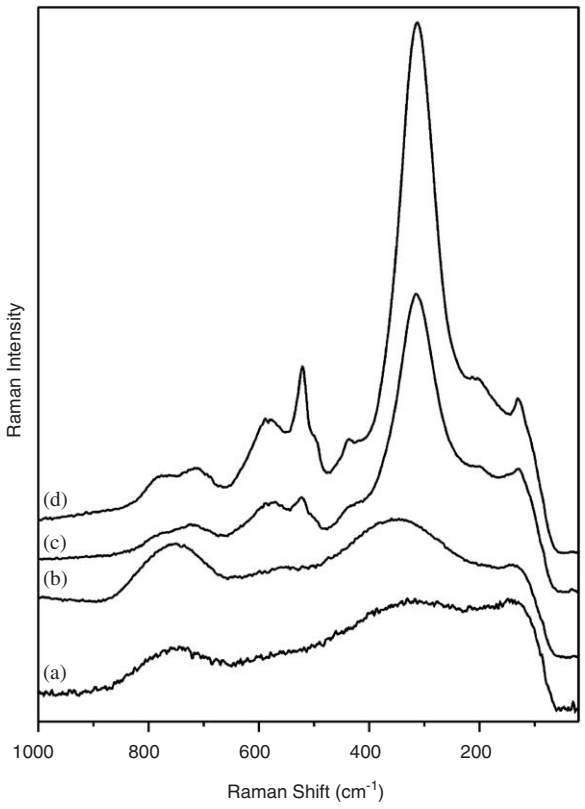

Fig. 3. Raman spectra obtained for the $Gd_2(Ti_{0.65}Zr_{0.35})_2O_7$ series of samples: just-milled (a) and milled and fired 12 h at 600 (b), 1000 (c) and 1200°C (d).

which also suggest the existence of a fluorite atomic arrangement for powders fired at temperatures of up to 800 °C with significant changes observed in those collected for samples treated at 1000 and 1200 °C. In particular, new bands appear at 712, 520 and 436 cm^{-1}, which undoubtedly point to the formation of a pyrochlore-type of structure. The presence of these bands is a clear indication of a phase transformation on $Gd_2(Ti_{0.65}Zr_{0.35})_2O_7$ when firing above 800 °C. Interestingly, the band near 750 cm^{-1} remains present after firing the sample at 1200 °C although is much weaker and narrower suggesting the presence of residual oxygen disordering even at this temperature. It is also clear that there are some differences between the pyrochlore samples fired at 1000 and 1200 °C; i.e. the Raman spectrum of the latter shows higher intensity of the 520 cm^{-1} band, lower intensity of the band near 750 cm^{-1} and smaller bandwidth of the 430 cm^{-1} band when compared with the sample fired at 1000 °C. These changes indicate that the ordering process is continuous, involving not only the metal substructure but also the oxygen one.

3.3. Microstructural characterization

As discussed above, mechanochemically prepared pyrochlore materials have a complex microstructure that cannot be accounted for by the conventional models. To study the microstructure of these compounds we have used the two-step procedure proposed by Langford [16–18]. As expected, due to the method of synthesis used, our samples present significant residual microstrains which became evident in the Williamson–Hall plots [21] (plot of β vs. d^*, not shown) obtained for the different samples. When microstrains are present, the integral breadth of the reflections are dependent on the order, i.e. are d^*-dependent. In these cases, the reflection integral breadths are due to both the size and the microstrains effects. According to Langford [16] and Halder et al. [22], it is possible to separate both contributions by using [1]:

$$(\beta/d^*)2 = \varepsilon^{-1}\beta/(d^*)^2 + (\eta/2)^2, \quad (1)$$

where is the ε gives the mean apparent domain size and η is a measure of the strain related with the root mean square strain (e_{rms}) by $e_{rms} \sim \eta/5$ [17]. The graphic representation of Eq. (1) is the so-called Langford plot of the sample. As an example, Figs. 4a and b show these plots for the as-prepared $Gd_2(Ti_{0.10}Zr_{0.90})_2O_7$ sample after firing 12 h at 400 °C and for the $Gd_2(Ti_{0.65}Zr_{0.35})_2O_7$ sample fired 12 h at 1200 °C, respectively. Applying Eq. (1) to the experimental data and assuming a spherical (isotropic) shape of the domains (which seems to be plausible due to the cubic symmetry of the materials) we obtained the values of the isotropic diameter, $\langle D_{iso} \rangle$, and the root mean square strain, e_{rms}, collected in Tables 1–3. From those values, it seems that the strains induced in the samples as a consequence of milling are difficult to relax; only at high temperature (1200 °C) the strain decreases significantly being essentially the same for the just milled samples and

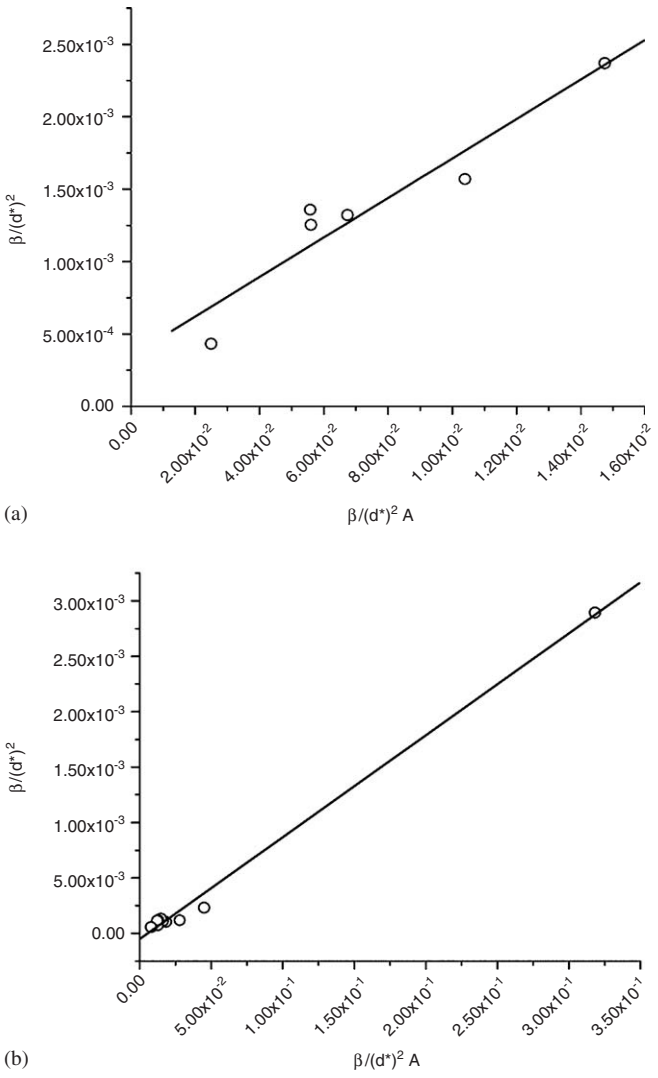

Fig. 4. Langford plots for the $Gd_2(Ti_{0.10}Zr_{0.90})_2O_7$ powder sample after firing for 12 h at 400 °C (a), and for the $Gd_2(Ti_{0.65}Zr_{0.35})_2O_7$ sample after firing for 12 h at 1200 °C (b).

for those heat treated up to 1000 °C. On the contrary, the domain size varies gradually with the firing temperature (almost like an exponential growth as observed for many temperature-activated processes); thus no abrupt change occurs in the domain size for any temperature suggesting the absence of a crystallization process from a more or less amorphous matrix. Interestingly, the thermal energy applied to the samples in the fluorite-like series of composition $Gd_2(Ti_{0.10}Zr_{0.90})_2O_7$ is only consumed in domain growth; as a result relatively large domains are produced at high temperatures (see Table 1). On the contrary, in the other two series of samples with higher Ti content and above a given temperature, the fluorite-to-pyrochlore structure transformation described above competes with domain growth yielding domains of smaller sizes than expected (Tables 2 and 3).

Thus, results presented in this work suggest that the as-prepared phases are metastable materials very far from the equilibrium state. Irrespective of their Zr content, they present a highly disordered atomic array which could be progressively ordered if enough energy (thermal in this case) during enough time is supplied to the samples. The metal rearrangement seems to be a "smooth" and slow process, in which heavy and highly charged ions have to reach their "natural" location within the structure with the final result of having the smaller Ti and Zr ions placed at the center of the BO_6 trigonal antiprisms as expected and the large Gd^{3+} cations in the eight-coordinated sites. On the basis of all the structural information collected in Tables 1–3, a two step process can be proposed to operate in the cation rearrangement responsible for the thermally induced metastable defect fluorite-to-pyrochlore transformation: first all the Ti ions would migrate to the hexa-coordinated sites by mainly displacing Zr^{4+} to the eight-coordinated positions and second, operating at higher temperatures, heavy Gd^{3+} cations would migrate from the octahedral sites to the large eight-coordinated ones forcing Zr ions to return to the 16*d* positions. Thus, the Zr ability to occupy both eight- and six-coordinated positions is crucial for this phase transformation to proceed. Even after thermal treatment at 1200 °C, the as-prepared powder phases do not seem to be equilibrium materials since significant amounts of Ti and/or Gd cations are located in the "wrong" sites. It is worth mentioning that gadolinium atoms in unusual coordination environments are not unknown. Thus, at least two different polymorphs of Gd_2O_3 are known: a high-temperature monoclinic *B*-Gd_2O_3 (>1200 °C) and a low-temperature cubic *C*-Gd_2O_3, both with Gd^{3+} atoms in atypical coordination. While in the first one Gd atoms are coordinated by 7 oxygen atoms, in the cubic form there would be only 6 surrounding each metal atom located at 6 corners of a cube. In fact, the structure of the *C*-form is also that of α-Mn_2O_3 and it might be derived, as pyrochlores, from that of fluorite by removing a quarter of the anions and then rearranging the atoms slightly [23]. Interestingly enough, there are also a few examples of Gd^{3+} atoms in octahedral coordination as in double perovskites such as Ba_2GdSbO_6 and Ba_2GdRuO_6 [24,25]. As we have reported previously [11], RE^{3+} cations can also occupy the 16*d* sites of the structure, the degree of occupation being governed by the rare-earth ions size. Thus, in $RE_2Ti_2O_7$ pyrochlores prepared by mechanical milling (*RE* = Y, Gd, Dy), the smaller Y^{3+} ($r^{VI} = 0.89$ Å) and Dy^{3+} ions ($r^{VI} = 0.91$ Å) [19] occupy the hexa-coordinated site to a much larger extent that the bigger Gd^{3+} ions (only about 5–10% of gadolinium ions were found to occupy the BO_6 trigonal antiprisms in $Gd_2Ti_2O_7$) although the present data suggest cation distribution among the 16*d* and 16*c* positions to be also governed by the size of the B^{4+} ions. However, the presence of seven-coordinated Ti atoms indicated by Raman spectroscopy and the chemical and structural flexibility of the pyrochlore structure suggest the detailed mechanism for the phase transformation observed in samples prepared by mechanical milling, to be a much

more complex scenario than that depicted above. The structural flexibility of the pyrochlores is such that the O(2)A_2 substructure (O(2) = oxygen atoms in 8*a*) can be partially occupied or even completely absent from the structure, as in the WO_3 pyrochlore-type polymorph [26]. In fact, the existence of a pyrochlore intrinsic structural feature, displacive disorder, has been suggested allowing small *B*-cations to occupy the large *A*-site of the structure [26]. This occurs through combined displacements of the *A* and O(2) atoms which changes the coordination of the *A*-site from 8 to (5 + 3) allowing smaller cations, such as Zn^{2+} in $Bi_{1.5}Zn_{0.92}Nb_{1.5}O_{6.92}$ ($r^{VI}(Zn^{2+}) = 0.74$ Å), to achieve a chemically reasonable environment in that position while retaining the cubic symmetry of the structure. As for the title solid solution, the structural integrity of the pyrochlore structure has been suggested to be based largely on the corner-shared distorted BO_6 octahedral network with the chemically induced structural disordering being dominated by changes in the local Gd^{3+} environment [9]. Thus, with increasing Zr content the nearest-neighbor oxygen shell coordinating the Gd^{3+} atoms changes progressively, from a pyrochlore-like environment (c.n. 8) to that characteristic of a defect fluorite with 1/8 anion vacancies (average cation-oxygen coordination numbers are between 6 and 8) to accommodate Zr substitution on the B site. According to these authors, the nearest-neighbor oxygen shell coordinating the B cation remains relatively unaffected. However, different studies carried out on the structural properties of the Gd_2O_3–ZrO_2 system [27–29], have suggested the existence of similar local arrangements around the Gd^{3+} ions in pyrochlore and fluorite-type $Gd_2Zr_2O_7$, i.e. the coordination number of Gd^{3+} remains fundamentally constant. Then, the fluorite structure would not be made up from the disordered system but of pyrochlore microdomains within a fluorite matrix. A hybrid phase model consisting of an intergrowth of domains with pyrochlore and defect fluorite structures has been proposed to explain the gradual transition between both forms of $Gd_2Zr_2O_7$, with the presence of anti-phase domain boundaries causing a broadening of the diffraction peaks of the pyrochlore superstructure prior to the phase transformation.

Thus, it seems that the final atomic configuration adopted by pyrochlore oxides is extremely dependent not only on chemical composition but also of the method chosen to process the powders under study and their thermal history with the extremely slow rate of cation diffusion in fluorite-related stabilized zirconia-based materials responsible to a great extent, for differences in the degree of ordering (disordering) between samples [30]. This point is further supported by the fact that $Gd_2Zr_2O_7$ samples prepared by mechanical milling using the same procedure described in the *Experimental* section are fluorites, even after treated at temperatures up to 1200 °C ($a = 5.2602(1)$ Å) as opposed to $Gd_2Zr_2O_7$ powders prepared by traditional solid state reaction which as mentioned before, present a pyrochlore-type of structure up to 1500 °C [10].

4. Conclusions

We have shown in this work the feasibility of preparing metastable fluorite-type of structures in the $Gd_2(Ti_{1-y}Zr_y)_2O_7$ solid solution, by mechanically milling constituent oxides. Post-milling thermal treatments allow some ordering processes to take place, the temperature needed to initiate it increasing as the Zr content increases. Thus, the composition with the highest Zr content, $Gd_2(Ti_{0.10}Zr_{0.90})_2O_7$, does not present the long-range atomic ordering characteristic of pyrochlores at any temperature with the fluorite-type of structure persisting even after firing the sample 12 h at 1200 °C. On the other hand, temperatures higher than 800 °C are needed to drive the Ti-rich composition, $Gd_2(Ti_{0.65}Zr_{0.35})_2O_7$, to the thermodynamically equilibrium pyrochlore structure although this one is really never reached and a small percentage of cation antisite defects remains present even after firing the sample at 1200 °C. Surprisingly, intermediate pyrochlore oxides with very unusual cation distribution appear during the thermally activated ordering process for both, $Gd_2(Ti_{0.35}Zr_{0.35})_2O_7$ and $Gd_2(Ti_{0.65}Zr_{0.35})_2O_7$, featuring Gd atoms distributed between the 6- and 8-coordinated positions and the Zr atoms relegated to the larger *A* site.

Acknowledgments

Financial support from Mexican Conacyt (SEP-2003-C02-44075) and Spanish CICYT (Project MAT2004-03070-C05-01) is greatly appreciated.

References

[1] J.S. Benjamin, Metall. Trans. 1 (1970) 2943.
[2] P.G. McCormick, F.H. Froes, JOM-J. Miner. Metall. Mater. Soc. 50 (1998) 61.
[3] B.J. Wuensch, K.W. Eberman, C. Heremans, E.M. Ku, P. Onnerud, E.M.E. Yeo, S.M. Haile, J.K. Stalick, J.D. Jorgensen, Solid State Ionics 129 (2000) 111.
[4] A.P. Ramirez, A. Hayashi, R.J. Cava, R. Siddharthan, B.S. Shastry, Nature 399 (1999) 333.
[5] J. Snyder, J.S. Slusky, R.J. Cava, P. Scheffer, Nature 413 (2001) 48.
[6] W.J. Weber, R.C. Ewing, Science 289 (2000) 2051.
[7] M. Subramanian, G. Aravamudan, G.V. Subba Rao, Prog. Solid State Chem. 15 (1983) 55.
[8] P.K. Moon, H.L. Tuller, Solid State Ionics, G. Nazri, R.A. Huggins, D.F. Shriver, (Ed), Mater. Res. Soc. Proc. 135 (1989) 149.
[9] N.J. Hess, B.D. Begg, S.D. Conradson, D.E. McCready, P.L. Gassman, W.J. Weber, J. Phys. Chem. B 106 (2002) 4663.
[10] D. Michel, M. Perez y Jorba, R. Collongues, Mater. Res. Bull. 9 (1974) 1457.
[11] A.F. Fuentes, K. Boulahya, M. Maczka, J. Hanuza, U. Amador, Solid State Sci. 7 (2005) 343.
[12] J. Lian, J. Chen, L.M. Wang, R.C. Ewing, J.M. Farmer, L.A. Boatner, K.B. Helean, Phys. Rev. B. 68 (2003) 134107.
[13] K.J. Moreno, R. Silva-Rodrigo, A.F. Fuentes, J. Alloy Compd. 390 (2005) 230.

[14] J. Rodriguez-Carvajal, Physica B 19 (1993) 55; See also a report in CPD of IUCr, Newsletter 2001, 26, 12; available at 〈http://www.iucr.org/iucr-top/comm/cpd/Newsletters〉. The program and manual can be found at 〈http://www-llb.cea.fr/fullweb/powder.htm〉
[15] S. García-Martín, M.A. Alario-Franco, H. Ehrenberg, J. Rodríguez-Carvajal, U. Amador, J. Am. Chem. Soc. 126 (2004) 3587.
[16] J.I. Langford, NIST Special Publication 846. Proceedings of the International Conference "Accuracy in Powder Diffraction II", Gaithersburg, MD, USA, 1992.
[17] J.I. Langford, Defect and Microstructure Analysis by Diffraction, in: P. Snyder, F. Fiala, H. Bunge (Eds.), IUCr Monographs on Crystallography, vol. 10, Oxford University Press, Oxford, 1999, pp. 59–81.
[18] D. Louër, Defect and Microstructure Analysis by Diffraction, in: P. Snyder, F. Fiala, H. Bunge (Eds.), IUCr Monographs on Crystallography, vol. 10, Oxford University Press, Oxford, 1999, pp. 671–697.
[19] R.D. Shannon, Acta Crystallogr. A 32 (1976) 751.
[20] M. Glerup, O.F. Nielsen, F.W. Poulsen, J. Solid State Chem. 160 (2001) 25.
[21] G.K. Williamson, W.H. Hall, Acta Metall. 1 (1953) 22.
[22] N.C. Halder, C.N. Wagner, J. Adv. X-ray Anal. 9 (1966) 91.
[23] A.F. Wells, Structural Inorganic Chemistry, 3rd Ed, Oxford University Press, London, 1962.
[24] H. Bader, S.Z. Kemmler-Sack, Z. Anorg. Allg. Chem. 466 (1980) 97.
[25] P. Garcia Casado, A. Mendiola, I. Rasines, Z. Anorg. Allg. Chem. 510 (1984) 194.
[26] T.A. Vanderah, I. Levin, M.W. Lufaso, Eur. J. Inorg. Chem. 14 (2005) 2895.
[27] T. Moriga, A. Yoshiasa, F. Kanamaru, K. Koto, M. Yoshimura, S. Somiya, Solid State Ionics 31 (1989) 319.
[28] A.J. Burggraaf, T. van Dijk, M.J. Verkerk, Solid State Ionics 5 (1981) 519.
[29] T. Uehara, K. Koto, F. Kanamaru, H. Horiuchi, Solid State Ionics 23 (1987) 137.
[30] Y. Liu, R.L. Withers, L. Norén, J. Solid State Chem. 177 (2004) 4404.